NORDA Technical Note 220

Naval Ocean Research and
Development Activity,
NSTL, Mississippi 39529

Assessment of Potential SSM/I Ice Products in Light of ESMR and SMMR Ice Classification Algorithms

Duane T. Eppler

Ocean Science and Technology Laboratory
Oceanography Division

June 1983

CONTENTS

ABSTRACT

The Special Sensor Microwave/Imager (SSM/I) will be launched aboard a DMSP satellite in FY-85. Seven channels of passive microwave data will be provided by the sensor at frequencies of 19.35 GHz, 22.235 GHz, 37.0 GHz, and 85.5 GHz. Dual polarizations will be measured in all but the 22.235 GHz channel where only the vertically polarized radiation will be sensed. Pixel size is dependent on frequency and ranges from approximately 55 km square at 19.35 GHz to less than 15 km square at 85.5 GHz. Spatial resolution of the high frequency 85.5 GHz channel is substantially better than the highest resolution obtained from ESMR and SMMR sensors (approximately 30 km). Data received from this channel will improve the accuracy with which ice edges and bodies of open water within the pack can be located. The cell size for which total ice concentration can be estimated also will be reduced. However, estimates of multi-year ice concentration, concentration of thin ice types, and the character of ice in the marginal ice zone will not be improved over SMMR estimates by virtue of these higher frequency data. Enhanced estimates of these parameters must come from development of improved ice classification algorithms. Improved ground truth information from which satellite data can be interpreted and verified is critical if classification algorithms are to be improved. Specifically, data that document radiometric signatures of wet and snow-covered ice surfaces that occur during summer and autumn months are needed to improve estimates of multi-year concentrations during melt and freeze-up. Brightness temperature data that describe the transition from open water to thick first-year ice are required for improved discrimination of thin ice types. Ground truth data that correlate marginal ice zone conditions with low-resolution imagery from satellite-borne microwave sensors are needed to improve estimates of conditions within the marginal ice zone.

ACKNOWLEDGMENTS

This work was performed during FY-83 under Satellite Oceanography Tactical Applications (SOTA) program element 63704, Al Pressman program manager, Capt. Dave Honhart, U.S. Navy, (OP-952) sponsor. NORDA coordinator was Jeff Hawkins of the Remote Sensing Branch. Critical readings by Jeff Hawkins and Dick Ketchum (NORDA Polar Oceanography Branch) improved the manuscript.

LIST OF SYMBOLS

Variables:

C	concentration within the satellite footprint
E	emissivity
T_B	brightness temperature in Kelvins
T_o	physical temperature in Kelvins
t_2	time at which maximum open water is reached
t_3	time at which freeze-up is complete
t	atmospheric opacity

Subscripts:

a	atmosphere
f	first-year
horz	horizontal polarization
i	ice
m	multi-year
n	channel designator for multichannel instrument
s	surface within the satellite footprint
sp	free space
vert	vertical polarization
w	open water

INTRODUCTION

Data obtained from satellite-borne imaging microwave radiometers are relevant to academic and applied problems in polar regions. As all-weather day-night sensors, they provide coverage of Arctic and Antarctic regions regardless of surface conditions. Information concerning sea ice concentration and age, daily configuration of the ice edge, location of polynyas, movement of ice masses and weather systems, and estimates of heat exchange between ocean and atmosphere in polar regions is derived from these data.

Launch of the Special Sensor Microwave/Imager (SSM/I) in 1985 aboard the DMSP satellite will provide a new source of all-weather, all-light images of the polar regions. Projected launches of consecutive SSM/I's on DMSP platforms and the Navy Remote Ocean Sensing System (NROSS) platform at the end of the decade present the possibility of nearly continuous polar coverage for the next ten years. Potential benefits accrued from these sensors will be reaped in the operational, tactical, academic, and research communities. Development of new analysis procedures that result could lead to significant improvements in estimating ice conditions in the marginal ice zone, more accurate predictions of multi-year ice concentrations during summer and autumn months, better assessment of heat balance parameters in ice covered regions, and a significantly improved understanding of basin-scale dynamics of the Arctic pack.

HISTORICAL DEVELOPMENT: ESMR-SMMR-SSM/I

The Electrically Scanning Microwave Radiometer (ESMR-5) was launched aboard Nimbus-5 in December 1972 to provide maps of precipitating clouds over ocean areas and to chart the distribution of sea ice in polar regions (Sabatini, 1972). ESMR utilized a single frequency (19.35 GHz) passive microwave radiometer with a beam width of 1.4° x 1.4° at nadir. The instrument employed a phased array antenna to scan 50° either side of the sub-satellite point. A 2500 km wide swath was included in each scan. Microwave images returned by the sensor are composed of brightness temperatures measured at each of 78 positions across the scan. Spatial resolution of these images is 25 km x 25 km at nadir, and degrades to 160 km crosstrack x 45 km downtrack at the ends of the scan. Polar coverage was virtually continuous due to the wide swath width; overlap between successive passes covered approximately 50% of latitudes above 70°. ESMR-5 functioned well until 1976 when certain beam positions in the phased array antenna were lost. As late as 1980 ESMR-5 was the primary source of data used to compile Navy operational ice analyses (Wilheit,

1980). An expanded discussion of the ESMR instrument is given by Wilheit (1972).

During its four year effective life, ESMR-5 returned data that established the value of satellite-borne microwave imagers to polar studies. Numerous workers have shown that diverse information concerning total sea ice concentration (Gloersen, et al., 1974, 1978; Campbell, et al., 1980; Comiso and Zwally, 1982; Carsey, 1982), multi-year ice concentration (Carsey, 1982), configuration of the ice edge (Gloersen, et al., 1974; Carsey, 1982), location of polynyas (Zwally and Gloersen, 1977; Rayner and Howarth, 1979; Carsey, 1980), and changes in the structure and character of the Arctic ice pack with time (Campbell, et al., 1980) is contained in ESMR-5 imagery. ESMR-5's primary weakness was its single-channel capability. Real-time discrimination of first-year ice from multi-year ice requires that radiation at several frequencies be compared. Furthermore, lack of accurate information regarding atmospheric effects that can be obtained from multi-channel radiometers limits the precision with which concentration estimates can be determined from the single-channel ESMR sensor.

ESMR-6, a successor to ESMR-5, was launched aboard Nimbus-6 in June 1975. The ESMR-6 instrument was designed as a multi-channel sensor and measured brightness temperatures at 37 GHz in both horizontal and vertical polarizations. Failure of the horizontal channel in September 1976 reduced ESMR-6 to a single-channel sensor. Although data obtained by ESMR-6 are potentially useful for mapping the extent of ice coverage and discriminating between first-year and multi-year ice types, ESMR-6 data largely have not been used in polar studies.

The Scanning Multichannel Microwave Radiometer (SMMR) flown aboard the Nimbus-7 (Nimbus-G) and Seasat-A satellites in 1978 was designed to rectify weaknesses inherent in the ESMR instrument. Technology associated with the Nimbus ESMR, Microwave Spectrometer (NEMS), and Scanning Microwave Spectrometer (SCAMS) were incorporated into SMMR design (Gloersen and Barath, 1977). The SMMR instrument measures microwave radiation through ten channels at five frequencies. Passive radiation is sensed in both vertical and horizonatal polarizations at 6.633, 10.69, 18.0, 21.0, and 37.0 GHz. For the 37 GHz channels, two radiometers are used, one for each polarization. At each of the other four frequencies a single radiometer alternates between polarizations on sucessive scans. The angle of view for the instrument is 42° which, in the case of Seasat-A, produced a swath width of 595 km. Cell dimensions for a single pixel depend upon channel frequency and vary from 149 km x 149 km at 6.6 Ghz to an optimum 27 km x 27 km at 37 GHz for Seasat-A. The instrument aboard Nimbus-7 is forward viewing with the swath centered on the subsatellite track. The Seasat-A instrument was aft viewing with

the swath center 22° from nadir to the right of the satellite to permit overlap with footprints of the onboard scatterometer and synthetic aperture radar. Both Nimbus-7 and Seasat-A were launched in 1978. Seasat-A operated for 95 days from July 6 to October 10. Operation ceased when the onboard power system failed. Nimbus-7 has functioned from 1978 to present. Technical discussions of SMMR characteristics are presented by Gloersen and Barath (1977), Dunne (1978), Barrick and Swift (1980), Njoku, et al. (1980a, 1980b), and by Swanson and Riley (1980).

Improved spectral resolution offered by the multi-channel SMMR instruments permitted development of algorithms that significantly enhance ice concentration prediction capabilities (Gloersen, et al., 1981a, 1981b; Svendsen, et al., 1983). Real-time multi-year ice concentration, a quantity that could not be calculated daily from ESMR data, is calculated to an accuracy of ±10% from SMMR data. Total ice concentration estimates are accurate to ±3% under ideal conditions (Svendsen, et al., 1983). Location of the ice edge can be estimated to within ±10 km. However, detail within the marginal ice zone can not be resolved due to the large 30 km square footprint of the highest frequency channel. For similar reasons, many tactically significant bodies of open water can not be delineated.

The Special Sensor Microwave/Imager (SSM/I) will be launched aboard the DMSP satellite in FY-85. Seven channels of passive microwave data at frequencies of 19.35 GHz, 22.235 GHz, 37.0 GHz, and 85.5 GHz will be provided. Both vertical and horizonal polarizations will be measured in all but the 22.235 GHz channel where only vertically polarized data will be sensed. The effective footprint size ranges from 55 km for the low frequency 19.35 GHz channel to 15 km for the high frequency 85.5 GHz channel. Spatial resolution provided by the 85.5 GHz channel is improved significantly over SMMR and should provide refined estimates of ice edge locations. Polynyas of smaller size than previously seen in ESMR and SMMR imagery should be seen in SSM/I images. Accuracy of ice concentration estimates is projected by Hughes, Inc. to be ±12%. Ice edges are expected to be located to ±12.5 km. In light of accuracies achieved with SMMR data, SSM/I estimates should exceed these projections, especially after algorithms are tuned with ground truth data.

ICE CONCENTRATION ALGORITHMS

Evolution of passive satellite sensors has been accompanied by development of data processing techniques and procedures that extract information from radiometric signals. Raw radiometer data are reduced using a series of algorithms that perform calibration and analytic functions. Noise is removed, radiome-

tric corrections are made, and brightness temperatures are computed. The products of these algorithms typically are values of ice concentration, commonly total ice concentration but sometimes multi-year and firstyear ice concentrations as well. Generally the information is presented in map form. Algorithms exist to treat both single-channel ESMR data (Gloersen, et al., 1974, 1978; Zwally, et al., 1979; Carsey, 1982; Comiso and Zwally, 1982) and multi-channel SMMR data (Gloersen, et al., 1981a, 1981b; Martin, et al., 1982; Cavalieri, et al., 1983; Svendsen, et al., 1983).

The ability to estimate ice characteristics from microwave data is based on the fact that radiation emitted by ice and water is described by the Rayleigh-Jeans approximation for the intensity of thermal radiation emitted by a blackbody (Wilheit, 1972):

$$T_B = ET_o \qquad (1)$$

where T_B is the measured brightness temperature in Kelvins, E is the emissivity of the imaged material, and T_o is the absolute physical temperature of the material. The approximation assumes that the radiating medium is non-scattering and isotropic.

Ice-laden seas present complex surfaces in which several different media are contained within a single satellite-scale footprint. A given scene typically consists of open water in the form of leads, polynyas, or open seas, first-year ice and new ice of various thicknesses, and floes composed of thick, low-salinity multi-year ice. Each of these materials possesses different physical characteristics. The assumption of isotropy thus is violated. Atmospheric moisture, atmospheric emission, and emission from free space further contribute to total brightness temperatures sensed by a satellite-borne imager and compound the problem (Fig. 1). Equation 1 must therefore be rewritten to account for each medium imaged in a given footprint:

$$\begin{aligned} T_B = {} & E_m T_{om} C_m && \text{(multi-year component)} \\ & + E_f T_{of} C_f && \text{(first-year component)} \\ & + T_{Bw} C_w && \text{(open water component)} \\ & + T_{Ba} && \text{(atmospheric contribution)} \end{aligned} \qquad (2a)$$

where C is the fraction of the footprint that a particular component encompasses such that:

$$C_m + C_f + C_w = 1 \qquad (2b)$$

The total brightness temperature sensed thus is a linear combination of the relative proportions of each component in the footprint.

Atmospheric contributions are functions of absorption of radiation emitted from the surface, largely by water vapor (atmospheric opacity), and emission of radiation from the atmosphere itself. Atmospheric effects typically are small at the poles due to low humidity conditions characteristic of the region (Wilheit, et al., 1972). This is especially true during winter months. At lower latitudes in the vicinity of marginal ice zones, open water is extensive and warmer physical temperatures increase the capacity of the atmosphere to hold water. Here, atmospheric attenuation is greater and its contribution to brightness temperature limits the sensitivity of uncorrected brightness temperature measurements to a larger degree. Variation in atmospheric water with latitude, season, weather, and with the location of the marginal ice zone means that the effects of atmosphere can not be described adequately by a single correction factor applied consistently, or even regionally, to brightness temperature measurements.

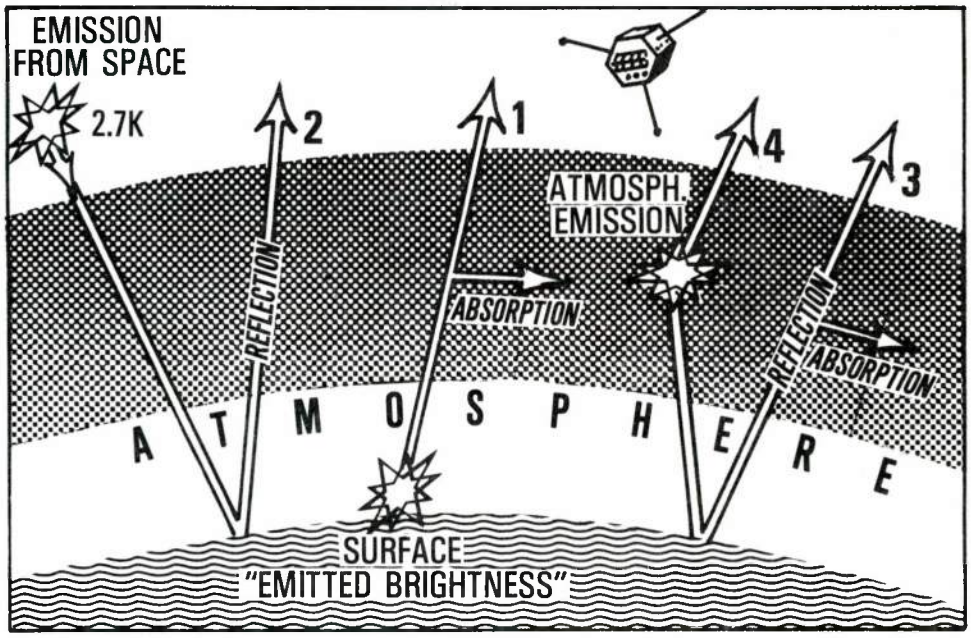

FIGURE 1. Sources of microwave radiation received by satellite sensors (Svendsen, et al., 1983). Brightness temperature is a function of four components: (1) emitted brightness from the surface, (2) radiation from space reflected by the surface, (3) upwelling radiation from the atmosphere, and (4) downwelling atmospheric radiation reflected from the surface.

Computation of the atmospheric correction from radiometric data requires that multi-channel instruments0be used. Insufficient degrees of freedom are present in single-channel data to resolve the atmospheric component. Atmospheric effects commonly are assumed to be negligible in ESMR ice algorithms; the loss of precision that results is included in the overall error of the sensor and the algorithm. With multi-channel data, models of atmospheric effects independent of surface effects can be developed (Svendsen, et al., 1983). The potential accuracy of algorithms that utilize multi-channel data thus is enhanced.

ESMR Algorithms

The single-channel character of ESMR data places limitations on the amount of information it contains. Real-time algorithms that utilize ESMR data generally are unable to discriminate between first-year and multi-year ice. Delayed analysis of seasonal data does, however, yield multi-year ice concentration measurements (Carsey, 1982). The general operational utility of ESMR sensors lies in their proven ability to map the ice edge and to estimate first-year ice concentrations in the absence of multi-year ice. The simplicity of non-iterative, real-time models permits reasonably accurate ice forecasts to be made with only modest computational capability.

Real-time Algorithms

If multi-year ice is assumed to be absent from the imaged scene (a valid assumption in Antarctic waters and in the Bering Sea) and if the atmospheric contribution to brightness temperatures sensed by the satellite is assumed to be negligible, then Equation 2 can be simplified to include only the first-year and open water components:

$$T_B = E_f T_{of} C_f + T_{Bw} C_w \qquad (3a)$$

With multi-year ice absent, the brightness temperature of a scene is assumed to be a linear combination of C_f, the area covered by first-year ice, and C_w, the area covered by open water:

$$C_f + C_w = 1 \qquad (3b)$$

The concentration of first-year ice in such a two component system, then, is given by:

$$C_f = \frac{T_B - 135}{E_f T_{os} - 135} \qquad (3c)$$

where T_B is the measured brightness temperature of the scene as sensed by the satellite radiometer, 135 is the brightness temperature of open water in Kelvins, and T_{os} is the physical temperature of the ice surface (Zwally, et al., 1979; Comiso and Zwally, 1982). Conversely, the proportion of the footprint that consists of open water is given by Gloersen, et al. (1974) as:

$$C_w = \frac{T_B - E_f T_{os}}{135 - E_f T_{os}} \qquad (3d)$$

Equations 3c and 3d form the basis of non-iterative algorithms devised to produce maps of first-year ice concentration from ESMR brightness temperatures.

The accuracy of values used to initialize the algorithm, specifically the emissivity of first-year ice (E_f) and physical surface temperature (T_{os}), also limit the accuracy of predictions based on the algorithm. Furthermore, where more than one ice type is present, uncertainty in the relative proportions of first-year ice, new ice types, and multi-year ice introduce errors. Early attempts to deduce ice concentration in the Arctic basin from single-channel ESMR data typically failed to account for new ice. Actual concentrations of ice in the central basin typically were higher than those predicted from Equation 3c as a result of the influence of radiometrically colder new ice and multi-year ice. Because ESMR's accuracy is limited by the presence of multiple ice types within the satelite footprint, its utility is highest in the Antacrtic where the multi-year concentration within the pack typically is small and the location of multi-year ice and shelf ice can be predicted accurately (Gloersen, et al., 1981b).

Overall accuracy for the model is estimated to be $\pm$6% for ice concentration greater than 35% (Gloersen, et al., 1974) and $\pm$10% or better overall (Gloersen and Salomonson, 1975). These estimates are not documented by ground truth data. Carsey (1982) sets the lower limit of ice concentration that can be detected accurately in the marginal ice zone from ESMR data at 15% when weather conditions are unknown. Ocean roughness, foam, high concentrations of atmospheric water vapor, and suspended water droplets associated with the occurrence of severe weather effectively increase the brightness temperature of open water to that of a calm sea with 15% ice concentration. Reliable concen-

tration estimates below 15% total sea ice thus can not be made unless accurate weather information is available.

Delay-time Algorithms

Carsey (1982) presents a different approach to analysing ESMR data that yields estimates of the fixed multi-year ice concentration within a frozen pack during a given winter. Estimates of multi-year ice obtained from the algorithm are determined by measuring the total amount of open water present at the end of summer melt. Ice that survives summer melt becomes multi-year ice upon freeze-up. By determining the maximum percentage of open water at late summer within a given area the percentage of winter multi-year ice present within that same area also is known. In order to determine the maximum open water area, analysis of ESMR brightness temperatures over the entire freeze period is required. Instantaneous, real-time estimates of multi-year ice concentration can not be obtained from ESMR data for this reason.

Carsey divided the Arctic Basin into quadrants 200 km on a side. ESMR brightness temperature values for pixels within each quadrant were averaged on each day of the 90 day period between August 12 and November 10, 1974. During this period both maximum open water at the end of summer and complete freeze-up at the close of the Arctic autumn occur. Daily brightness temperatures then were plotted as a function of time for the entire period for each quadrant. The point at which maximum open water occurs is correlative with the minimum brightness temperature observed over this interval for each grid element. The point at which all open water is frozen (total freeze-up) is marked by the maximum brightness temperature observed. The general pattern displayed by each grid element consists of a minimum brightness temperature (maximum open water) during the period August 27 to September 17. This is followed by a gradual increase to a maximum T_B at the end of October. Attainment of this maximum is interpreted as an indication that freezing of open water is complete. If the proportion of multi-year ice within each grid element is assumed to be constant throughout the freeze-up period, differences in the minimum and maximum brightness temperatures observed between grid quadrants is a function of the relative proportion of multi-year ice within each quadrant (Carsey, 1982). Carsey thus computes the concentration of multi-year ice (C_m) and the emissivity of multi-year ice (E_m) within a given grid element as functions of minimum and maximum brightness temperature:

$$C_m = \frac{E_s(t_3) - E_s(t_2) + \frac{T_{Bw}}{T_{om}(t_2)} - \frac{E_f T_{of}(t_3)}{T_{om}(t_3)} + D\left[\frac{1-E_w}{T_{om}(t_2)} - \frac{1-E_f}{T_{om}(t_3)}\right]}{d\left[1 - \frac{D}{T_{om}(t_2)}\right] + \frac{T_{Bw}}{T_{om}(t_2)} - \frac{E_f T_{of}}{T_{om}(t_2)} + D\left[\frac{E_f}{T_{om}(t_3)} - \frac{E_w}{T_{om}(t_2)}\right]} \quad (4a)$$

and

$$E_m = \frac{E_s(t_3) - (1-C_m)\frac{E_f T_{of}}{T_{om}(t_3)} - \frac{D[1-E_f(1-C_m)]}{T_{om}(t_3)}}{C_m\left[1 - \frac{D}{T_{om}(t_3)}\right]} - \frac{d}{2} \quad (4b)$$

where $T_{om}(t_2)$ is the minimum physical surface temperature reached in a given quadrant (the physical temperature on the day of maximum open water) and $T_{om}(t_3)$ is the maximum physical surface temperature reached during the summer-winter transition (the physical temperature on the first day of complete ice cover). D is a correction for atmospheric radiance.

Carsey's equations provide delayed estimates of multi-year ice concentration for large (200 km) quadrants of the Arctic basin on the basis of single-channel data taken over the period from maximum open water (middle to late August) to freeze-up (middle to late October). Neither instantaneous estimates of multi-year concentration, nor estimates of multi-year concentrations during late spring and early summer can be obtained directly from single-channel data (ESMR) using equations 4a and 4b. However, the amount of summer multi-year ice present in a given year probably can be estimated from the previous winter's multi-year cover. If the concentration of multi-year ice remaining at the end of the summer is calculated, and if the rate of change from spring to fall is assumed to be linear (or some well-behaved function of climate), then the multi-year concentration in a specific quadrant can be estimated after accounting for drift of ice from the previous year's quadrants.

Numeric estimates of the accuracy of multi-year ice concentrations computed from the algorithm are not provided. Instead, Carsey (1982) makes a qualitative assessment of potential sources of error involved in the analysis. Variance in the emissivity of multi-year ice is assessed as the factor that introduces the

greatest variation. Conditions at the ice surface change rapidly during summer melt and autumn freeze-up of the pack. Occurrence of rain and wet snow in conjunction with diurnal freezing and thawing of water in the top centimeters of ice cause dramatic fluctuations in emissivity. Although radical changes in brightness temperature that result are well documented (Carsey, 1982; Ketchum, 1982), relationships between imaged brightness temperatures and specific surface conditions that they indicate are poorly understood. The existence of surface conditions that give deceptively cold temperatures near the time of maximum open water or deceptively warm temperatures when freezing is nearly complete would cause values of $T_{om}(t_2)$ and $T_{om}(t_3)$ to be chosen incorrectly.

A second source of error is drift of ice through each quadrant over the three month period of freeze-up. The large grid size (200 km square) was chosen such that areal extent of ice that remains within a given quadrant for the entire period would be large compared the amount of ice that enters and leaves the quadrant as a result of drift. At the same time, the grid size could not be so large that several different ice regimes would be encompassed within each quadrant. Patterns in the fluctuation of brightness temperatures observed within individual quadrants are similar to those observed in adjacent quadrants. This suggests that similar ice conditions prevail over regions of areal extent larger than the size of each quadrant (Carsey, 1982). Furthermore, changes in ice character from one region to another are transitional rather than abrupt, suggesting that the algorithm will remain robust even if abnormally high drift rates move large quantities of ice through adjacent quadrants.

SMMR Algorithms

Algorithms that employ SMMR multi-channel data are based on the premise that emissivities of different imaged media (open water, first-year and multi-year ice, atmospheric water), though similar at some microwave frequencies, are different at other frequencies. Thus, although multi-year ice can not be adequately discerned from first-year ice at the ESMR frequency (19.35 GHz), first-year and multi-year ice are characterized by different emissivities at other frequencies. The multi-channel capability of SMMR instruments enhance the accuracy of ice concentration predictions significantly. Effects of multi-year ice and atmospheric radiance and opacity can be accounted for and their influence on predicted total ice concentrations mediated or corrected. Severe problems still exist, however, in transitional seasons when emissivities of wet and freezing surfaces are in constant flux.

Non-iterative Algorithms

Martin, et al. (1982) and Cavalieri, et al. (1983) present a two-channel, non-iterative algorithm that derives estimates of first-year ice concentration from radiation at the 37 GHz frequency. The method uses polarization differences in emissivity between open water and first-year ice to map the concentration of first-year ice. Ice concentration is given by:

$$C_f = \frac{1}{(1-R)} \tag{5a}$$

where

$$R = \frac{T_{Bf(horz)} - \frac{(1-PR)}{(1+PR)} T_{Bf(vert)}}{T_{Bw(horz)} - \frac{(1-PR)}{(1+PR)} T_{Bw(vert)}} \tag{5b}$$

and

$$PR = \frac{T_{B(vert)} - T_{B(horz)}}{T_{B(vert)} + T_{B(horz)}} \tag{5c}$$

C_f is the computed concentration of first-year ice in the satellite field of view, $T_{Bf(horz)}$ and $T_{Bf(vert)}$, and $T_{Bw(horz)}$ and $T_{Bw(vert)}$ are known brightness temperatures for consolidated first-year ice (no open water) and water in horizontal and vertical polarizations, and $T_{B(horz)}$ and $T_{B(vert)}$ are the measured brightness temperatures of the satellite field of view for the horizontal and vertical channels. The model assumes that atmospheric contributions to imaged brightness temperatures are negligible.

Martin, et al. (1982) estimate possible errors of up to 24% for ice concentration predictions using this model. The 24% figure is based on ground truth data acquired during field experiments in the Bering Sea. The algorithm assumes that only first-year ice is present (a valid assumption for the Bering Sea). However, the algorithm does not discriminate thin first-year ice from open water. This is the largest source of error. Lower concentrations than actually are present are given for areas with significant concentrations of thin first-year ice. Furthermore, the overall accuracy of the algorithm is dependent

on the emissivity of imaged ice types being close to the tuned values of T_{Bf} and T_{Bw} used in the algorithm. Factors such as salinity, surface roughness, and surface temperature are judged to be less important than the presence of ice of a single radiometric type (Martin, et al., 1982). Results obtained compare favorably with ice edge and concentration maps produced independently from Tiros data and field data, although estimates near landfall are not as accurate.

NORSEX Algorithm

Svendsen, et al. (1983) present an iterative algorithm used during NORSEX that predicts both multi-year and first-year ice concentration from two channels of vertically polarized data. The 37 GHz SMMR channel is used in conjunction with either the 18 Ghz or the 10.7 GHz channel, depending on the accuracy and spatial resolution desired. Values needed for atmospheric corrections are extracted from appropriate SMMR channels and applied to the total brightness temperature sensed by the satellite before contributions of the ice-water surface are determined.

Raw brightness temperatures measured by the satellite first are calibrated with respect to cold and warm radiators over areas of open ocean and first-year ice for which brightness temperatures are known. Prelaunch calibration data and polarization demixing procedures are used as well. Accuracy of the NORSEX algorithm depends in large part on the accuracy of these calibrated values. Next, an atmospheric correction based on work by Gloersen and Barath (1977, eq. 1) is made:

$$T_{Bs} = \frac{T_B - 2dT_a t_a + dT_a t_a^2 - T_{sp}}{1 - t_a - bd(t_a - t_a^2) - b\frac{T_{sp}}{T_a}} \qquad (6a)$$

where T_{Bs} is the corrected brightness temperature contributed by the imaged ice-water surface (atmospheric effects removed), T_B is the brightness temperature measured by the satellite (surface brightness temperature plus atmospheric effects), t_a is the total atmospheric opacity (optical depth from Reeves, 1975), T_{sp} is the temperature of free space, approximately 2.7 K, and b and d are constants given values of 0.95 and 0.90 respectively. The term dT_a is the weighted average atmospheric temperature in the lower troposphere.

With an approximation of atmospheric effects removed, equations 2a and 2b are solved for a three component system of multi-year ice, first-year ice, and open water using two channels of data:

$$T_B = C_m E_m T_{oi} + C_f E_f T_{oi} + C_w E_w 272 \quad (6b)$$

T_{oi}, the effective physical temperature of the imaged ice surface, is a function of air and ocean temperature and is approximated by:

$$T_{oi} = aT_{oa} + (1-a)272 \quad (6c)$$

where T_{oa} is the physical air temperature at the surface, 272 is the physical ocean temperature, and a is estimated from field data to be approximately 0.40. Initial values for atmosphere temperature (Equation 6c, T_{oa}) are derived from the best available surface source (ice camps, airborne PRT-5 and PRT-6 instruments, and automated ice buoys drifting within the pack).

Brightness temperatures measured by two SMMR channels are used in Equation 6b to yield two equations with two unknowns. These are solved to give initial concentrations of multi-year and first-year ice (C_m and C_f). Next, refined values for optical opacity (t_a) and atmospheric brightness temperature (T_{Ba}) are determined. T_{Ba} is found from the initial values of C_f and C_m by interpolating between a brightness temperature for 100% open water and the measured brightness temperature for 100% ice concentration. The refined t_a is found using this new value of T_{oa}. Finally, Equations 6a and 6b are solved using these new estimates of T_{Ba} and t_a to produce final values of C_f and C_m.

Based on field data acquired during NORSEX in a test area between Greenland and Svalbard, the NORSEX algorithm estimates total ice concentration to $\pm$3% and the multi-year concentration to $\pm$10% under ideal conditions (Svendsen, et al., 1983). Comparison of measurements of total ice concentration derived from aircraft ground truth data with concentrations derived with the NORSEX algorithm show a mean difference of 0.5$\pm$5% using the 10/37 GHz SMMR combination. Absolute accuracy of total concentration derived from aircraft is $\pm$3%. Accuracy of -3.5$\pm$2% was achieved using the 18/37 GHz combination, meaning that the SMMR algorithm estimates concentration an average of 3.5% too low. Accuracy of multi-year ice concentration estimates are -4.0$\pm$6% for the 10/37 GHz combination, and -8.0$\pm$6% for the 18/37 GHz

combination. Absolute aircraft accuracy for predicting multi-year concentration is ±10%. The presence of very thin first-year ice or meltponds on multi-year ice force larger errors. Wet snow on multi-year ice, a common phenomenon during summer and autumn seasons, causes multi-year ice to appear warmer, like first-year ice. Spatial resolution of 90 km is achieved when the 10 GHz and 37 GHz channels are combined; 60 km resolution is achieved using the 18 GHz and 37 GHz channels.

Gloersen Algorithm

Gloersen, et al. (1981a, 1981b) present an algorithm for determining values of four variables from eight channels of SMMR satellite data. Total ice concentration (C), multi-year concentration (F), sea ice temperature (T_{oi}), and atmospheric liquid water (L) are derived using the vertically and horizontally polarized brightness temperatures of the 4.6, 2.8, 1.4, and 0.8 cm SMMR channels. Brightness temperature is assumed to be the sum of four discrete sources:

$$\begin{aligned}\text{Brightness Temperature} = {} & \left.\begin{array}{l}\text{(Surface Emissivity)}\\ \text{x (Phys. Surface Temp)}\\ \text{x (Atmos. Absorption)}\end{array}\right. + \left.\begin{array}{l}\text{(Upwelling}\\ \text{Atmos. Rad.)}\end{array}\right. + \\ & \left.\begin{array}{l}\text{(Refl. Downwelling}\\ \text{Atmos. Radiation) x}\\ \text{(Atmos. Absorption)}\end{array}\right. + \left.\begin{array}{l}\text{(Refl. Space Rad.) x}\\ \text{(2 x Atmos. Absorp.)}\end{array}\right.\end{aligned}$$

Or, in algebraic terms:

$$T_{Bn} = E_n T_{oi} e^{-t_n} + \left.\begin{array}{l} T_1 + (1-E_n)T_2 e^{-t_n} \\ + (1-E_n)T_{osp} e^{-2t_n}\end{array}\right\} \quad \begin{array}{l}\text{Atmospheric}\\ \text{Correction}\\ \text{Terms}\end{array} \qquad (7a)$$

where:

$$E_n = E_{wn}(1-C) + E_f(1-F-X)C + E_m FC + E_f XC \qquad (7b)$$

T_{Bn} is the brightness temperature sensed by the satellite through channel n, E_{wn} is the emissivity of the ocean at the frequency of channel n, E_f and E_m are the emissivities of first-year and multi-year ice at this same frequency, T_{oi} is the physical temperature of the ice surface, T_{osp} is the physical temperature of open space, X is the thin first-year ice fraction of C, T_1 and T_2 are physical atmospheric temperatures and t is the atmospheric opacity.

Gloersen, et al. (1981a) assume that for polar regions T_1 and T_2 are approximately equal to a weighted atmospheric temperature of the lower troposphere which is approximately equal to the temperature of the ice surface. On the basis of this assumption and others that concern the relatively small opacity of the polar atmosphere, Equation 7a is converted to:

$$\begin{aligned} T_{Bn} = {} & 268E_{wn}(1-C) + E_f(T_{oi}-3)C \\ & - (E_f-E_m)(T_{oi}-3)FC \\ & - (E_f-E_{ft})(T_{oi}-3)XC \\ & + E_{ft}(T_{oft}-T_{oi})XC \\ & + \frac{2.384L}{l_n^2}\left[T_{oi}-271E_{wn}(1-C)-E_f t_i C(1-F)-E_m T_{oi}CF\right] + 3 \end{aligned} \qquad (7c)$$

where 271 is the physical ocean temperature in Kelvins, E_{ft} is the difference between the emissivity of first-year ice and first-year thin ice, and l_n is the wavelength of channel n.

Initially, Gloersen, et al. (1981a) sought to solve Equation 7c simultaneously for six unknowns: the four given above (C, F, T_{oi}, and L) plus the thin first-year ice fraction of C (X) and the difference between thick and thin ice temperature. However, high correlations between brightness temperatures recorded for adjacent channels produced unacceptably high noise factors for many parameters. The revised algorithm solves iteratively for C, T_{oi}, L, and F. T_{oi}, L, and F are solved at a resolution of 156 km; C is solved at a scale of 25 km. Pre-launch values for E_o, E_f, E_m, ant E_{ft} are used to initialize Equation 7c. The algorithm shown in Figure 2 is followed to compute the above variables. Convergence typically occurs in approximately five iterations (Gloersen, et al., 1981a).

Gloersen, et al. (1981a) claim to achieve some rather remarkable accuracies with their algorithm. Total ice concentration at a 156 km scale is estimated to be $\pm$4% after the first iteration, and as good as $\pm$1% after several iterations. Total

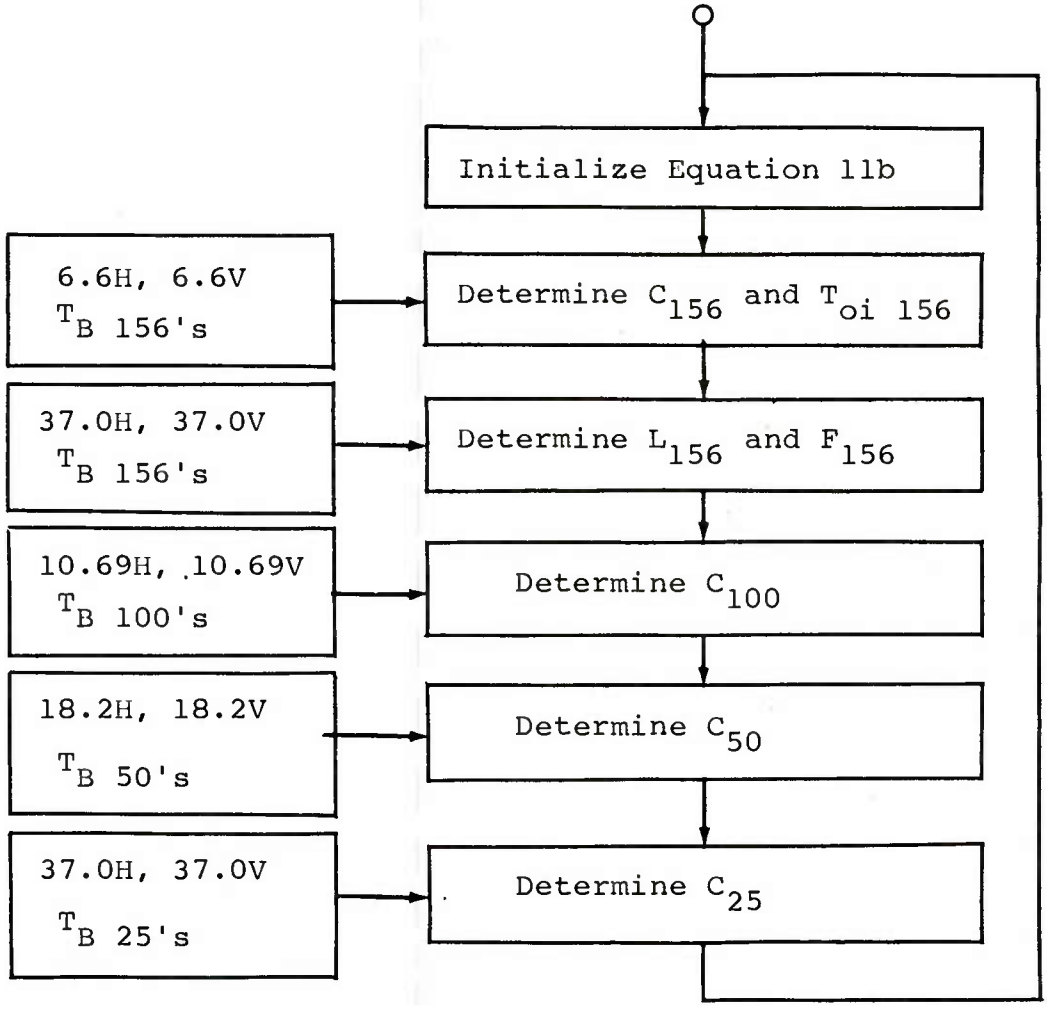

FIGURE 2. Algorithm for determining total ice concentration (C), sea ice temperature (T_{oi}), atmospheric liquid water (L), and multi-year ice concentration (F) from SMMR data (Gloersen, et al., 1981a). Brightness temperatures txat are input and the size of their footprints are given in boxes to the left. Parameters shown to the right are derived at resolutions indicated from these inputs using Equations 7a through 7c (see text).

concentrations at the 100, 50, and 25 km scales after iterating are estimated to be ±2, 3, and 5%. Physical ice temperature is estimated to an accuracy of 9 K initially, and 3 K ultimately at the 156 km scale. Atmospheric liquid water is estimated to ±0.015 cm (±0.011 cm with iteration) and the multi-year fraction of total ice concentration to ±24% (±19% after iterating), also at the 156 km scale. Ground truth data to support these accuracy estimates are not presented by Gloersen, et al. (1981a, 1981b).

SSM/I IMPACT ON ICE ANALYSIS

SMMR and ESMR products provide indications of the minimum accuracy and versatility that can be expected from SSM/I data. They also expose weaknesses in currently used analysis strategies that should be strengthed before the next generation of satellite imagery is available. Review of past work is instructive when viewed in this light. If improved estimates of ice pack characteristics are to be extracted from SSM/I data, then improved data analysis techniques must be developed and implemented. Previous applications for satellite-borne microwave imagery fall into four general categories: (1) ice concentration, (2) location of the ice edge and characteristics of the marginal ice zone, (3) location of polynyas, large leads, and open water, and (4) estimates of heat exchange in polar regions. The state of each is assessed below.

Ice Concentration

Estimates of ice concentration based on ESMR and SMMR data are derived from algorithms described above. SMMR algorithms should be applicable to SSM/I data with alterations to accomodate differences in frequency. The SMMR sensor suite includes radiometers at 10, 18, 21, and 37 GHz; SSM/I will carry radiometers at 19, 22, 37, and 85 GHz. Emissivities of multi-year and first-year ice at 85 GHz are similar to those at 37 GHz, the high frequency channel aboard SMMR instruments (Fig. 3) (Troy, et al., 1981). The improved spatial resolution that 85 GHz offers (14.8 km vs. 33 km) will enhance the quality of SSM/I products that are based primarily on this sensor: location of the ice edge and determination of total ice concentration in the absence of multi-year ice. Therefore, data from the 85.5 GHz channel should be utilized in computing these variables. Discrimination between thick first-year ice and new ice or thin first-year ice, however, is ambiguous at 85 GHz (Troy, et al., 1981). Use of high frequency channels in conjunction with lower resolution, lower frequency channels will be necessary to discern first-year ice

thicknesses and to compute multi-year ice concentrations. Spatial resolution for these estimates could be as poor as 55 km if data from the 19 GHz channel are utilized.

Ice concentration estimates derived from SSM/I data will be comparable in accuracy to those attained using SMMR imagery. Svendsen, et al. (1983) present the best documented SMMR algorithm estimates (NORSEX). Total concentration is estimated to ±3% and multi-year ice concentrations are estimated to accuracies of ±10% using the 10 GHz and 37 GHz vertical channels combined. These errors are based on ground truth data and represent figures for optimum conditions. Where very thin ice is present or where meltponds occur, errors will be larger in the absence of ground truth data. Furthermore, multi-year ice covered by wet snow will appear as first-year ice and increase the error of multi-year concentration estimates (Svendsen, et al., 1983).

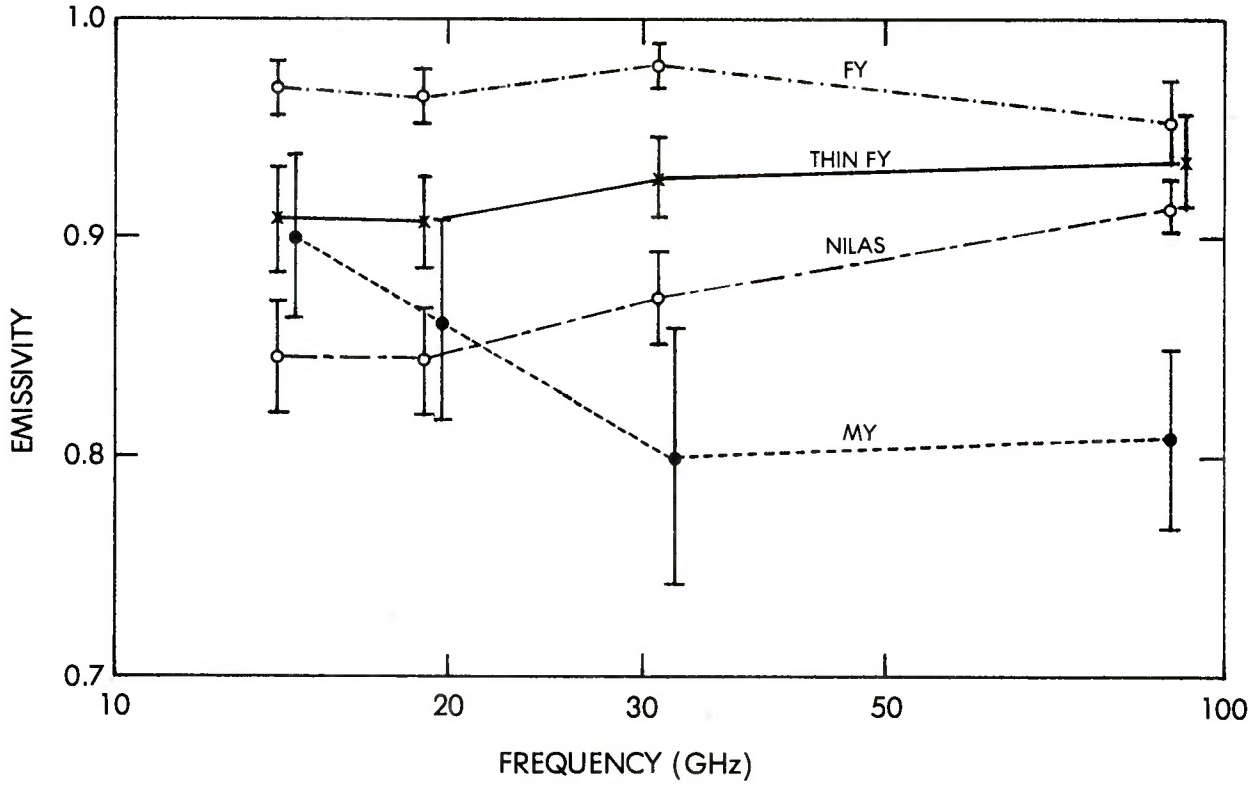

FIGURE 3. Emissivity as a function of frequency between 14 and 90 GHz for four ice types (from Troy, et al., 1981). Vertical bars mark one standard deviation from the plotted mean.

In general, the accuracy of concentration estimates will not be improved by the higher-resolution sensor suite aboard SSM/I. Although exclusive use of the 85 GHz channel to estimate total ice concentration will reduce pixel size (area) by approximately 75%, errors in approximating actual concentrations within each cell will be unaffected. The accuracy of a given estimate is largely a function of the algorithm by which it is produced. Only by improving analysis procedures will the accuracy of estimates be increased.

The ultimate accuracy of any ice classification algorithm is determined principally by three factors: (1) the information content of the raw data, (2) the ability of the algorithm to remove noise from the raw data, and (3) the ability of the algorithm to discern ice types on the basis of information contained in raw data from which noise has been removed. The information content of data gathered by a particular suite of sensors is dependent on radiometer frequencies and polarizations incorporated into design of the instrument. Characteristics of the instrument in effect set boundary conditions that determine the type of information that can be extracted as well as the upper limits of the quality of that information. Thus, the highest level of accuracy that can be obtained in predicting a given parameter is determined by innate characteristics of the sensor suite. The choice of sensors is invariant after the design freeze and is a fixed quantity that can not be altered. Improved accuracy of SSM/I data over SMMR data, then, will only be achieved to the extent that noise removal techniques can be enhanced and discrimination strategies that are used to recognize specific ice types are improved.

Noise, as used here, is a function of environmental factors that create differences between the brightness temperature perceived by the satellite sensor and energy actually emitted by the ice-water surface. Atmospheric opacity, atmospheric emission, emission from free space, and inaccurate calibration correction procedures are the primary sources of error associated with noise. Atmospheric corrections either are based on assumed values of atmospheric opacity and emission (Gloersen, et al., 1981a) or are determined iteratively from multi-channel data (Svendsen, et al., 1983). Some workers assume that atmospheric effects are minimal and fail to make any correction at all (Martin, et al., 1982; Cavalieri, et al., 1983). Such algorithms are neither as accurate nor as reliable as algorithms in which atmospheric effects are removed completely.

Calibration corrections are applied to raw data received from the satellite before processing by ice classification algorithms and also affect accuracy. Raw data received from the satellite are in the form of voltages that are proportional to differences between the sensed radiometric signal and internal

reference sources aboard the satellite (Swanson and Riley, 1980). Brightness temperatures are determined from these voltage data using calibration algorithms. Pre-launch data that describe the behavior of the instrument are used in conjunction with polarization demixing procedures to convert received voltages to brightness temperatures (Gloersen and Barath, 1977; Njoku, et al., 1980b; Swanson and Riley, 1980). Additional corrections based on measurements over warm and cold radiators of known value are used by some workers to increase further the accuracy of computed brightness temperatures (Svendsen, et al., 1983). Clearly, the accuracy of these corrections and calibrations is a critical factor in determining the ultimate accuracy with which ice parameters are estimated.

The ability of the algorithm to discern ice types from these corrected signals is a function of three factors: the overall discrimination strategy from which the algorithm is defined, the accuracy of values used to initialize iterative algorithms, and fundamental assumptions made regarding the type of materials present in the imaged field of view. Existing algorithms fail to describe summer and autumn conditions adequately. Fluctuations in the emissivity of summer snow-covered ice caused by changing weather conditions and diurnal freeze-thaw cycles are poorly understood. Accordingly, discrimination strategies are poorly formulated, assumptions concerning the radiometric appearance of imaged ice are violated, and seed values used to initialize certain algorithms are poorly chosen. Significant improvements in the overall performance of SSM/I algorithms can be made by formulating strategies designed to improve predictions of ice concentration during summer melt and autumn freeze-up.

Ice Edge and Marginal Ice Zone

A primary use of satellite remote sensing in arctic regions is location of the ice edge. Daily updates derived from microwave sensors provide information needed to keep ice charts current. Microwave imagery provided by ESMR and SMMR type instruments represent significant improvements over visible and infrared imagery in that they return images of the surface regardless of weather and light conditions. Accuracy in locating the edge is determined by sensor resolution and by ice and weather conditions at the ice edge. Differences between the emissivity of water and ice make the delineation of compact ice edges reasonably unambiguous. Dispersed edges are located less easily. The minimum ice concentration that can be detected reliably is 15% in the absence of accurate weather data regardless of sensor resolution (Carsey, 1982). An effective resolution of 30 km per square pixel is achieved by most microwave

imagers to date. SSM/I's 85.5 GHz channel with a footprint 14.8 km square should enhance our ability to locate the edge more accurately. SMMR accuracies comparable to or better than those achieved with Tiros data are reported by several workers (Martin, et al., 1982; Cavalieri, et al., 1983). Work performed by Svendsen, et al. (1983) in conjunction with NORSEX located the edge to within ±10 km from SMMR data. Improved accuracy of approximately 50% is expected of SSM/I based on the improved resolution of the 85.5 GHz channel.

Resolution of specific features within the marginal ice zone is achieved less easily. A change in brightness temperature of more than 60 K over a 100 km wide zone is required to insure that geographical averaging across the 30 km square ESMR field of view does not obscure features within the marginal pack (Carsey, 1982). As a consequence, detailed pictures of ice concentration have not been developed, even with SMMR data (Svendsen, et al., 1983). Nonetheless, some aspects of the character of ice within the zone can be deduced. SMMR sensors show differences in response between compact and dispersed edges making qualitative descriptions of ice conditions possible. Some indication of the type of ice present also is suggested (Svendsen, et al., 1983). Improved resolution offered by the 85.5 GHz SSM/I channel should permit improved concentration estimates to be made for the marginal ice zone. However, determination of ice age information is likely to remain out of reach as a result of the low resolution of lower frequency sensors needed to discern multi-year ice concentrations accurately.

Polynyas

Several groups of workers have studied large polynyas using ESMR imagery. Zwally and Gloersen (1977), Rayner and Howarth (1979), and Carsey (1980) report on the large (2×10^5 km^2) recurring polynya in the Weddell Sea offshore from Antarctica. Carsey (1980) monitored development and decay of the polynya through four winters. Changes in shape, location, and size were developed from ESMR images. Crawford and Parkinson (1981) monitored winter changes in the shape and size of North Water Polynya for three winter periods. Crane, et al. (1982) and Crane (1983) report relationships between late summer polynyas in the Arctic Basin and regional weather patterns. Cavalieri, et al. (1983) describe the development of large lee-shore polynas in the Bering Sea caused by the movement of pack ice past St. Matthew and St. Lawrence Islands. This last study used SMMR imagery and demonstrated that the location of such areas of low ice-concentration can be documented more accurately with SMMR imagery than with conventional Tiros data. The overall accuracy of locating

polynya boundaries is similar to accuracies involved in locating ice edges (±10 km, Svendsen, et al., 1983).

Each of these studies reports on large polynyas. Smaller features are difficult to detect using ESMR and SMMR sensors due to the poor instrument resolution. Many tactically significant leads and polynyas are likely to be smaller than the 15 km footprint of the highest frequency SSM/I sensor. Although averaging across footprints that contain large percentages of open water will produce differences between brightness temperatures seen in surrounding pixels, noise in the imaging system could easily mask subtle differences needed to detect tactically significant areas of open water reliably.

Integrated brightness temperature measurements carry insufficient information to determine the configuration of open water bodies contained within single pixels if conventional ESMR-SMMR analytic procedures described above are used. Brightness temperatures that indicate 50% open water could reflect a single circular polynya at the pixel center as well as an anastomosing network of narrow leads, the total area of which is 50% of the field of view. Image enhancement techniques that utilize multiple images of the same feature taken on successive orbits conceivably could be developed to reduce the clouding effects of signal noise and improve the reliability of single-pixel information.

Arctic Heat Exchange and Energy Balance

Carsey (1982) and Svendsen, et al. (1983) demonstrate the utility of using satellite derived microwave imagery to estimate heat exchange between ocean and atmosphere in polar regions. Changes in ice concentration are known to affect synoptic weather patterns (Ackley and Keliher, 1976; Carleton, 1981; Cavalieri and Parkinson, 1981; Crane, et al., 1982; Crane, 1983). Energy flux drives regional weather patterns and is a function of both the areal extent of insulating ice that covers warm ocean waters and the thickness of that cover. The concentration of multi-year ice present at a given time is used to determine these parameters. Both ESMR (Carsey, 1982) and SMMR (Svendsen, et al., 1983) data have been used.

Accurate data regarding multi-year ice covers, though difficult to obtain, are crucial to the accuracy of global models that forecast long term weather patterns (Carsey, 1982). When the total ice concentration is high, as it is during winter months, small errors in the estimate of total ice concentration result in large errors in the heat budget estimate. For example, a 3% error for total ice concentration of 85% produces a heat budget error of 15% (Maykut, 1978; Svendsen, et al., 1983). If

the actual total ice concentration is 95%, an error in the SMMR estimate of 3% produces an error of 50% in the heat exchange estimate. Improvement in accuracy of multi-year ice concentrations derived from SSM/I algorithms thus would represent a significant improvement in estimates of global heat balance.

CONCLUSIONS AND RECOMMENDATIONS

Imagery provided by the SSM/I sensor will represent marginal improvement over SMMR data, and significant improvement over ESMR data. Although resolution of the high frequency 85.5 GHz SSM/I channel is substantially greater than the 30 km resolution offered by SMMR's highest frequency, data received from this channel will affect the accuracy of only some ice analysis products. Spatial resolution of the position of ice edges and the location of open water within the pack will be improved. Further, the cell size for which total ice concentration can be estimated will be reduced. The 85.5 GHz channel should be used to compute these parameters. However, improvements in the accuracy with which multi-year ice concentration, the concentration of thin ice types, and the character of ice in the marginal ice zone are predicted must come from improvements in ice algorithms. Improved ground truth information from which satellite data can be interpreted and verified is critical if predictive capabilities are to be improved.

In this light, research that addresses the following points should be supported if the utility of ice analysis products is to be enhanced:

1. Information from the 85.5 GHz channel must be incorporated into existing algorithms to capitalize on the improved resolution that this sensor offers. The Hughes algorithm presently implemented at Fleet Numerical Oceanography Command (FNOC) facilites does not utilize data from this channel.

2. Current algorithms designed to treat SMMR data probably can be modified to accept SSM/I data, given the similarity of frequencies involved. It might be equally efficient to write new algorithms that overcome weaknesses of the SMMR algorithm suite discussed here. The approach generally taken in the past was to design one algorithm that provides estimates for all parameters. The possibility of developing specialty algorithms that yield better estimates of specific parameters from SSM/I data in conjunction with data from other satellite sensors should be explored.

3. Radiometric signatures of wet or snow-covered ice surfaces that occur during summer and autumn months are not well documented. Brightness temperature data from which predictive

algorithms can be written to discriminate multi-year ice from first-year ice during melt and freeze-up are needed.

4. Processing techniques that examine common areas viewed on separate orbital passes have not been applied to satellite-borne microwave imagery. Features that occur at scales near sensor resolutions might be enhanced if such techniques are implemented. Conditions within the marginal ice zone and tactically significant areas of open water and thin ice of areal extent smaller than can now be resolved might be identified from SSM/I images.

5. Ground truth data that correlate marginal ice zone conditions with imagery from satellite-borne microwave instruments are needed to improve estimates of conditions within the marginal ice zone. The possibility of developing specialty algorithms designed specifically to treat data within the marginal ice zone should be explored.

6. Current algorithms fail to discriminate adequately between thin ice types. Ground truth data that describe the transition from open water to thick first-year ice are needed.

REFERENCES CITED

ACKLEY, S.F., and KELIHER, T.E., 1976, Antarctic sea ice dynamics and its possible climatic effects: AIDJEX Bulletin 33, p.53-76.

BARRICK, D.E., and SWIFT, C.T., 1980, The Seasat microwave instruments in historical perspective: IEEE Journal of Oceanic Engineering, v.OE-5, n.2, p.74-79.

CAMPBELL, W.J., RAMSEIER, R.O., ZWALLY, H.J., and GLOERSEN, P., 1980, Arctic sea-ice variations from time-lapse passive microwave imagery: Boundary-Layer Meteorology, v.18, p.99-106.

CARLETON, A.M., 1981, Monthly variability of satellite-derived cyclonic activity for the southern hemisphere winter: Journal of Climatology, v.1, p.21-38.

CARSEY, F.D., 1980, Microwave observations of the Weddell Polynya: Monthly Weather Review, v.108, p.2032-2044.

CARSEY, F.D., 1982, Arctic sea ice distribution at the end of summer 1973-1976 from satellite microwave data: Journal of Geophysical Research, v.87, n.C8, p.5809-5835.

CAVALIERI, D.J., and PARKINSON, C.L., 1981, Large-scale variations in observed Antarctic sea ice extent and associated atmospheric circulation: Monthly Weather Review, v.109, p.2323-2336.

CAVALIERI, D.J., MARTIN, S., and GLOERSEN, P., 1983, Nimbus 7 SMMR observations of the Bering Sea ice cover during March 1979: Journal of Geophysical Research, v.88, n.C5, p.2743-2754.

COMISO, J.C., and ZWALLY, H.J., 1982, Antarctic sea ice concentrations inferred from Nimbus 5 ESMR and Landsat imagery: Journal of Geophysical Research, v.87, n.C8, p.5836-5844.

CRANE, R.G., 1983, Atmosphere-sea ice interactions in the Beaufort/Chuckchi Sea and in the European sector of the Arctic: Journal of Geophysical Research, v.88, n.C7, p.4505-4523.

CRANE, R.G., BARRY, R.G., and ZWALLY, H.J., 1982, Analysis of atmosphere-sea ice interactions in the Arctic Basin using ESMR microwave data: International Journal of Remote Sensing, v.3, n.3, p.259-276.

CRAWFORD, J.P. and PARKINSON, C.L., 1981, Wintertime microwave observations of the North Water Polynya, in Gower, J.F.R. (ed.), Oceanography From Space: Plenum Press, New York, p.839-844.

DUNNE, J.A., 1978, The experimental oceanographic satellite Seasat-A: Boundary-Layer Meteorology, v.13, p.393-404.

GLOERSEN, P., WILHEIT, T.T., CHANG, T.C., NORDBERG, W., and CAMPBELL, W.J., 1974, Microwave maps of the polar ice of the earth: Bulletin American Meteorological Society, v.55, n.12, p.1442-1448.

GLOERSEN, P. and SALOMONSON, V.V., 1975, Satellites -- new global observing techniques for ice and snow: Journal of Glaciology, v.15, n.73, p.373-389.

GLOERSEN, P., and BARATH, F.T., 1977, A scanning multi-sxannel microwave radiometer for Nimbus-G and SeaSat-A: IEEE Journal of Oceanic Engineering, v.OE-2, n.2, p.172-178.

GLOERSEN, P., ZWALLY, H.J., CHANG, T.C., HALL, D.K., CAMPBELL, W.J., and RAMSEIER, R.O., 1978, Time-dependence of sea-ice concentration and multiyear ice fraction in the Arctic basin: Boundary-Layer Meteorology, v.13, p.339-359.

GLOERSEN, P., CAVALIERI, D., and CAMPBELL, W.J., 1981a, Derivation of sea ice concentration, age and surface temperature from multispectral microwave radiances obtained with the Nimbus-7 scanning multi-channel microwave radiometer, in Gower, J.F.R. (ed.), Ocenaography From Space, Plenum Press, New York, p.823-829.

GLOERSEN, P., CAMPBELL, W.J., and CAVALIERI, D., 1981b, Global maps of sea ice concentration, age and surface temperature derived from Nimbus-7 scanning multi-channel microwave radiometer data: a case study, in Gower, J.F.R. (ed.), Oceanography From Space, Plenum Press, New York, p.777-783.

KETCHUM, R.D., 1982, SEASAT SAR sea ice imagery from summer melt to fall freeze-up: NORDA Technical Note 178, 12 p.

MARTIN, S., CAVALIERI, D.J., GLOERSEN, P., and McNUTT, S.L., 1982, The Bering Sea ice cover during March 1979: Comparison of surface and satellite data with the Nimbus-7 SMMR: U.S. Departmenv of Commerce Report, Contract MO-A01-78-00-4335, University of Washington, Seattle, 50p.

MAYKUT, G.A., 1978, Energy exchange over young sea ice in the central Arctic: Journal of Geophysical Research, v.83, n.C7, p.3646-3658.

NJOKU, E.G., CHRISTENSEN, E.J., and COFIELD, R.E., 1980a, The Seasat scanning multi-channel microwave rqdiometer (SMMR): antenna pattern corrections -- development and implementation: IEEE Journal of Oceanic Engineering, v.OE-5, n.2, p.125-137.

NJOKU, E.G., STACEY, J.M., and BARATH, F.T., 1980b, The Seasat scanning multi-channel misrowave radiometer (SMMR): instrument description and performance: IEEE Journal of Oceanic Engineering, v.OE-5, n.2, p.100-115.

RAYNER, J.N., and HOWARTH, D.A., 1979, Antarctic sea ice: 1972-1975: Geographical Review, v.69, n.2, p.202-223.

REEVES, R.G. (ed.), 1975, Manual of remote sensing: American Society of Photogrametry, Falls Church, Virginia.

SABATINI, R.R. (ed.), 1972, The Nimbus 5 user's guide: NASA Goddard Space Flight Center (U.S. Govt. Printing Office) 162p.

SVENDSEN, E., KLOSTER, K., FARRELLY, B., JOHANNESSEN, O.M., JOHANNESSEN, J.A., CAMPBELL, W.J., GLOERSEN, P., CAVALIERI, D., and MATZLER, C., 1983, Norwegian remote sensing experiment: evaluation of the Nimbus 7 scanning multi-channel microwave radiometer for sea ice research: Journal of Geophysical Research, v.88, n.C5, p.2781-2791.

SWANSON, P.N., and RILEY, A.L., 1980, The Seasat scanning multi-channel microwave radiometer (SMMR): radiometric calibration algoritho development and performance: IEEE Journal of Ocenaic Engineering, v.OE-5, n.2, p.116-124.

TROY, B.E., HOLLINGER, J.P., LERNER, R.M., and WISLER, M.M., 1981, Measurement of the microwave properties of sea ice at 90 GHz and lower frequencies: Journal of Geophysical Research, v.86, n.C5, p.4283-4289.

WILHEIT, T.T., 1972, The electrically scanning microwave radiometer (ESMR) experiment, in Sabatini, R.R. (ed.), The Nimbus 5 User's Guide: NASA, Goddard Space Flight Center (U.S. Govt. Printing Office), p.59-105.

WILHEIT, T.T., 1980, Microwave radiometry: NASA Technical Memorandum 80233, p. IV-11 to IV-13.

ZWALLY, H.J., and GLOERSEN, P., 1977, Passive microwave images of the polar regions and research applications: Polar Record, v.18, n.116, p.431-450.

ZWALLY, H.J., PARKINSON, C.L., CARSEY, F.D., GLOERSEN, P., CAMPBELL, W.J., and RAMSEIER, R.O., 1979, Seasonal variation of total Antarctic sea ice area, 1973-75: Antarctic Journal of the United States, v.14, n.5, p.102-103.

UNCLASSIFIED

SECURITY CLASSIFICATION OF THIS PAGE *(When Data Entered)*

REPORT DOCUMENTATION PAGE

READ INSTRUCTIONS BEFORE COMPLETING FORM

1. REPORT NUMBER: NORDA TECHNICAL NOTE 220	2. GOVT ACCESSION NO.
3. RECIPIENT'S CATALOG NUMBER	
4. TITLE *(and Subtitle)*: Assessment of Potential SSM/I Ice Products in Light of ESMR and SMMR Ice Classification Algorithms	5. TYPE OF REPORT & PERIOD COVERED: Final
6. PERFORMING ORG. REPORT NUMBER	
7. AUTHOR(s): Duane T. Eppler	8. CONTRACT OR GRANT NUMBER(s)
9. PERFORMING ORGANIZATION NAME AND ADDRESS: Naval Ocean Research and Development Activity, National Space Technology Laboratories, NSTL, Mississippi 39529	10. PROGRAM ELEMENT, PROJECT, TASK AREA & WORK UNIT NUMBERS: P.E. 63704
11. CONTROLLING OFFICE NAME AND ADDRESS: same	12. REPORT DATE: June 1983
	13. NUMBER OF PAGES: 32
14. MONITORING AGENCY NAME & ADDRESS *(if different from Controlling Office)*	15. SECURITY CLASS. *(of this report)*: UNCLASSIFIED
	15a. DECLASSIFICATION/DOWNGRADING SCHEDULE

16. DISTRIBUTION STATEMENT *(of this Report)*

Approved for public release, distribution unlimited.

17. DISTRIBUTION STATEMENT *(of the abstract entered in Block 20, if different from Report)*

18. SUPPLEMENTARY NOTES

19. KEY WORDS *(Continue on reverse side if necessary and identify by block number)*

DMSP	Ice	Age	Classification	Heat
ESMR	Concentration	Arctic	Microwave	Satellite
SMMR	Edge	Polar	Radiometer	Polynya
SSM/I	Algorithm			

20. ABSTRACT *(Continue on reverse side if necessary and identify by block number)*

The Special Senors Microwave/Imager (SSM/I) will be launched aboard a DMSP satellite in FY-85. Seven channels of passive microwave data will be provided by the sensor at frequences of 19.35 GHz, 22.235 GHz, 37.0 GHz, and 85.5 GHz. Dual polarizations will be measured in all but the 22.234 GHz channel where only the vertically polarized radiation will be sensed. Pixel size is dependent on frequency and ranges from approximately 55 km square at 19.35 GHz to less than 15 km square at 85.5 Ghz. Spatial resolution of the

DD FORM 1 JAN 73 1473 EDITION OF 1 NOV 65 IS OBSOLETE
S/N 0102-LF-014-6601

UNCLASSIFIED

SECURITY CLASSIFICATION OF THIS PAGE *(When Data Entered)*

high frequency 85.5 GHz channel is substantially better than the highest resolution obtained from ESMR and SMMR sensors (approximately 30 km). Data received from this channel will improve the accuracy with which ice edges and bodies of open water within the pack can be located. The cell size for which total ice concentration can be estimated also will be reduced. However, estimates of multi-year ice concentration, concentration of thin ice types, and the character of ice in the marginal ice zone will not be improved over SMMR estimates by virtue of these higher frequency data. Enhanced estimates of these parameters must come from development of improved ice classification algorithms. Improved ground thruth information from which satellite data can be interpreted and verified is critical if classification algorithms are to be improved. Specifically, data that document radiometric signatures of wet and snow-covered ice surfaces that occur during summer and autumn months are needed to improve estimates of multi-year concentrations during melt and freeze-up. Brightness temperature data that describe the transition from open water to thick first-year ice are required for improved discrimination of thin ice types. Ground truth data that correlate marginal ice zone conditions with low-resolution imagery from satellite-borne microwave sensors are needed to improve estimates of conditions within the marginal ice zone.